How to cite: *Angew. Chem. Int. Ed.* **2022,** *61,* e202206298
International Edition: doi.org/10.1002/anie.202206298
German Edition: doi.org/10.1002/ange.202206298

NMR Spectroscopy | Hot Paper

A Field-Independent Method for the Rapid Generation of Hyperpolarized [1-^{13}C]Pyruvate in Clean Water Solutions for Biomedical Applications

Salvatore Mamone, Anil P. Jagtap, Sergey Korchak, Yonghong Ding, Sonja Sternkopf, and Stefan Glöggler**

Abstract: Hyperpolarization methods in magnetic resonance enhance the signals by several orders of magnitude, opening new windows for real-time investigations of dynamic processes in vitro and in vivo. Here, we propose a field-independent para-hydrogen-based pulsed method to produce rapidly hyperpolarized ^{13}C-labeled substrates. We demonstrate the method by polarizing the carboxylic carbon of the pyruvate moiety in a purposely designed precursor to 24 % at ≈22 mT. Following a fast purification procedure, we measure 8 % polarization on free [1-^{13}C]pyruvate in clean water solutions at physiological conditions at 7 T. The enhanced signals allow real-time monitoring of the pyruvate-lactate conversion in cancer cells, demonstrating the potential of the method for biomedical applications in combination with existing or developing magnetic resonance technologies.

Nuclear magnetic resonance (NMR) is a powerful analytical tool for elucidating chemical compositions, structures and dynamics in molecules of biological interest. Magnetic resonance imaging (MRI) is a non-invasive imaging method that does not use ionizing radiations or radioactive tracers. Magnetic resonance (MR) technology is commonly used in chemical, biological and pharmaceutical laboratories and is becoming more widespread in clinics for in vivo diagnostics.

[*] Dr. S. Mamone, Dr. A. P. Jagtap, Dr. S. Korchak, Dr. Y. Ding, S. Sternkopf, Dr. S. Glöggler
Max Planck Institute for Multidisciplinary Sciences
NMR Signal Enhancement Group
Am Fassberg 11, 37077 Göttingen (Germany)
and
Center for Biostructural Imaging of Neurodegeneration of UMG,
NMR Signal Enhancement Group
Von-Siebold-Straße 3 A, 37075 Göttingen (Germany)
E-mail: salvatore.mamone@mpinat.mpg.de
stefan.gloeggler@mpinat.mpg.de

Hyperpolarization methods aim to expand the scope of MR by increasing the nuclear spin polarization by four orders of magnitude or more, allowing for the observation of low-sensitive spin labels at low concentrations and increased spatial and temporal resolutions. For example, MRI detects primarily water (H_2O), which is the most abundant component in living organisms (concentration ≈50 M). Metabolite signals are comparatively weaker since they are usually present at much lower concentrations (10 mM at most). The possibility of monitoring metabolism in real time using hyperpolarized (HP) probes has led to innovative methods to assess cancer aggressiveness and response to treatments in vitro as well as in vivo.[1–7]

Dissolution dynamic nuclear polarization (d-DNP) is the method of choice to attain large signal enhancements on ^{13}C-labeled metabolites.[8] In d-DNP, the high level of spin polarization residing on unpaired electrons at extremely low temperatures (0.8 K to 1.5 K) and high magnetic fields (3.3 T to 10 T) is transferred to the nuclear spins using microwave radiation. The build-up of polarization on the target nuclei requires tens of minutes typically. In order to use the HP probe for further applications, the sample is rapidly dissolved via suitably heated solutions. Despite high polarization levels, the widespread adoption of DNP-based methodologies is hampered by the need of cryogens, technical challenges and high associated costs.

A set of more accessible and portable hyperpolarization methods relies on the spin order residing in the para spin isomer of molecular hydrogen (para-H_2 in short).[9,10] Para-H_2 is produced by passing hydrogen gas over a catalyst at low temperatures. In absence of spin-converting catalysts, the spin isomer enrichment is preserved, allowing for para-H_2 to be stored and delivered on demand. Para-H_2-induced polarization (PHIP) manifests itself in considerable signal enhancements after hydrogenation of a suitable substrate.[11,12] The scope of PHIP has widened with the introduction of the side arm hydrogenation (SAH) method, in which a) a precursor undergoes hydrogenation with para-H_2 and b) spin order is transferred to a spin label in the target molecule and c) the HP substrate is released by cleaving off the sidearm.[13–18] In another (non-hydrogenative) modality of PHIP called SABRE, the target substrate, para-H_2 and a catalyst form a transient complex in which spin order flows to the nuclear spin of interest and hyperpolarization builds over the free substrate following such reversible exchanges.[19] To date, high polarization levels via

SABRE on ^{13}C metabolites in fully biocompatible solutions are still lacking, although recent advances appear promising.[20,21] In previous studies, we demonstrated that pulsed PHIP methods can lead to a high level of ^{13}C polarization (≈60 %) on metabolite precursors in the organic phase within few seconds in weakly coupled spin systems at high magnetic fields.[22–25] Such results have demonstrated that para-H_2-based methods can deliver ^{13}C polarization levels previously exclusive only to d-DNP.

In this article, we present a field-independent pulsed PHIP-SAH method for producing highly polarized metabolites in water at physiological conditions for biomedical applications. We demonstrate the method by polarizing [1-^{13}C]pyruvate in a portable system. Pyruvate is a crucial biomarker in cancer metabolism (aerobic glycolysis). Indeed, cancer cells preferentially convert pyruvate into lactate in the cytosol rather than using it in the three-carboxylic-acid (TCA) cycle inside the mitochondria, even in presence of oxygen.[26,27]

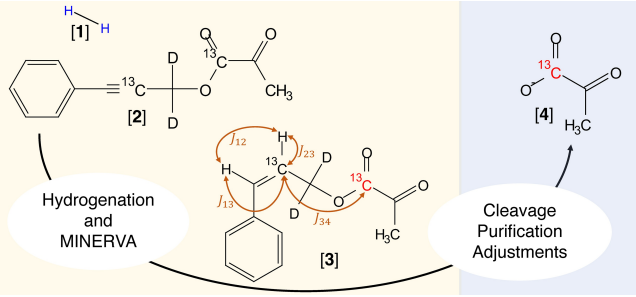

Figure 1. Scheme of the PHIP-SAH method used to obtain HP [1-^{13}C]pyruvate. Para-H_2 **[1]** is bubbled through an organic solvent solution containing a phenylpropynil pyruvate ester precursor (PPE in short) **[2]** and a homogeneous catalyst (not shown). Hydrogenation of the precursor leads to cis-cinnamyl pyruvate ester **[3]** (CPE in short). Using the MINERVA pulse sequence,[25] the spin order is transferred to the carbonyl ^{13}C nucleus of the pyruvate moiety via the highlighted *J*-couplings network ($J_{12} \cong 11.6$ Hz, $J_{13} \cong 0$ Hz, $J_{23} \cong 160$ Hz, $J_{34} \cong 2.3$ Hz). Following the cleavage of the ester bond, the removal of the organic solvent and the filtration of the catalyst, HP [1-^{13}C]pyruvate **[4]** is left in a neat biocompatible water solution, see main text for details.

The pulsed PHIP-SAH method is based on the following steps, see Figure 1:

1. *Hydrogenation*: para-H_2 **[1]** is bubbled through an organic solvent solution (here acetone-d_6) containing a phenylpropynil pyruvate ester precursor (PPE) **[2]** and a homogeneous catalyst, here [Rh(dppb)COD]BF_4;
2. *Spin Order Transfer*: after hydrogenation of the precursor, the para-H_2 spin order is transferred on an intermediate heteronucleus in the sidearm employing the relayed MINERVA (Maximizing Insensitive Nuclei Enhancement Reached Via para-H_2 Amplification) pulse sequence,[25] shown in figure 2a), and in turn is transferred to the ^{13}C-labeled moiety in the hydrogenated cis-cinnamyl pyruvate ester product (CPE) **[3]**. This methodology is named heteronuclear relayed PHIP-SAH.
3. *Cleavage*: a basic aqueous solution (here sodium carbonate) is added to cleave the ester bond.
4. *Purification and physiological adjustments*:
   4.1. a stripping gas (here nitrogen) is used to mix the solution, rapidly remove the solvent and precipitate part of the poor water-soluble catalyst leading to HP [1-^{13}C]pyruvate in water;
   4.2. the solution is mixed with a buffer solution (here PBS 2X at pH = 6.8) to achieve a solution with tonicity and pH within physiological ranges;
   4.3. after passing the solution through a micro-porous membrane filter to remove the catalyst, the biocompatible HP [1-^{13}C]pyruvate solution is ready for NMR/MRI applications.

The polarization transfer method presented here relies on the large *J*-couplings with a heteronucleus, to bring the

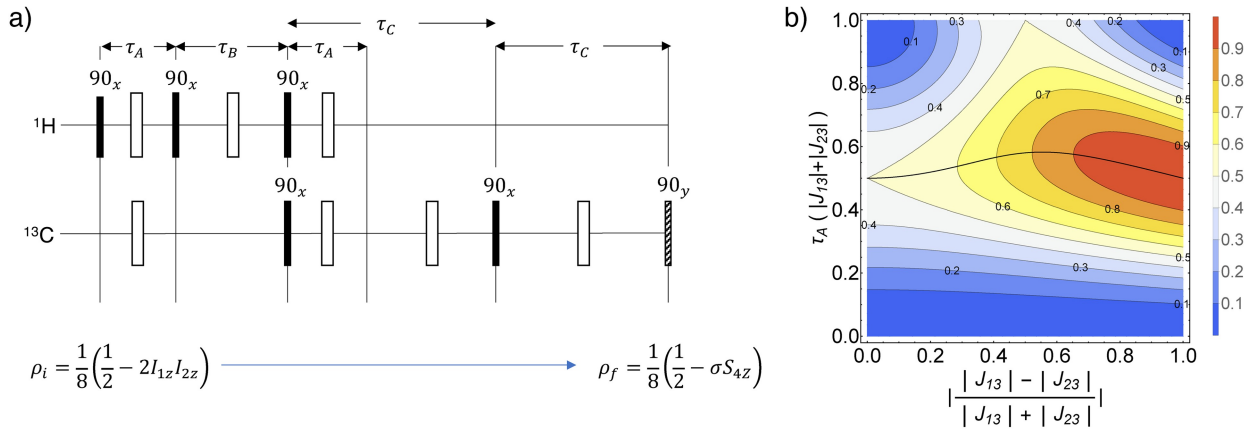

Figure 2. The pulse sequence used for polarization transfer is shown in panel a. The filled and open rectangles represent 90° and 180° pulses, respectively. The last dashed 90°-pulse on the ^{13}C channel is used to store the heteronuclear magnetization along the applied magnetic field but dropped for direct observation of the HP signal. The phases of the 180° pulses can be chosen at will along the transverse axes of the rotating radio-frequency frames, i.e. $\pm x$, $\pm y$. The sequence transfers PASADENA spin order $2I_{1z}I_{2z}$ into heteronuclear magnetization S_{4z} with efficiency σ, see Equation (2). Panel b is the contour plot of the efficiency σ in function of the heteronuclear *J*-couplings J_{13} and J_{23} and of the time τ_A at fixed $\tau_B = 0.5/|J_{12}|$ and $\tau_C = 0.5/|J_{34}|$. The black line crossing the plot tracks the maximal efficiency path.

spin system into the weakly coupled regime. Indeed, in the $^{13}C_2$-cis-cinnamyl pyruvate ester (CPE), Figure 1 **[3]**, the large one-bond coupling ($J_{23} \approx 160$ Hz) is used to achieve the initial PASADENA-type spin order $I_{1z}I_{2z}$ after incoherent hydrogenation with para-H_2 as well as weak coupling conditions suitable for the effective application of the MINERVA pulse sequence.[22–25] These conditions are valid in any magnetic field.

For the spin system (two ^{1}H and two ^{13}C) of the CPE molecule, Figure 1 **[3]**, the bridged MINERVA pulse sequence, shown in Figure 2a), transfers the two-spin longitudinal order $I_{1z}I_{2z}$ from the nascent para-H_2 via a bridge spin S_3 to heteronuclear magnetization on the spin of interest S_4. Following incoherent hydrogenation, the initial spin operator is $\rho_i = (0.5 - 2sI_{1z}I_{2z})/8$, where the spin order parameter $s = (4p-1)/3$ is linearly dependent on the para-H_2 fractional enrichment p. The relevant part of the spin order operator is transformed by the pulse sequence according to:

$$2I_{1z}I_{2z} \rightarrow \sigma \cdot S_{4z} \tag{1}$$

where the efficiency of the transfer in the weakly coupled approximation is:

$$\sigma = 0.5[1 - \cos(2\pi J_{12}\tau_A)\cos(2\pi J_{13}\tau_A)] \sin(\pi J_{12}\tau_B)[\sin(\pi J_{34}\tau_C)]^2 \tag{2}$$

leading to the final spin density operator $\rho_f = (0.5 - s\sigma S_{4z})/8$. A fully polarized heteronucleus is obtained when $s\sigma = 1$, which shows that the efficiency of the transfer sequence is as important as the para-isomer enrichment for achieving high polarization levels by PHIP. Figure 2b shows that the transfer efficiency is greater than 95 % when one of the heteronuclear couplings is much smaller than the other ($|J_{13}| < 0.1|J_{23}|$ or $|J_{23}| < 0.1|J_{13}|$), for $\tau_A \cong 0.5/(|J_{13}| + |J_{23}|)$, $\tau_B = 0.5/|J_{12}|$ and $\tau_C = 0.5/|J_{34}|$. It is worth noting that the efficiency is always greater than 50 % in the weak coupling approximation, independently of the heteronuclear couplings. Since in the $^{13}C_2$-CPE, Figure 1 **[3]**, $J_{12} \ll J_{23}$ and $J_{13} \ll J_{23}$, the spin system is in weak coupling conditions and the spin order transfer via MINERVA is expected to have close to 100 % efficiency *independently* of the applied field. The method is demonstrated in the following on a portable 22.6 mT electromagnet paired to a dual channel NMR console.[28]

Figure 3a shows the ^{13}C spectrum of the HP precursor after hydrogenation and spin order transfer at 22.6 mT. The frequency scale is relative to the ^{13}C Larmor frequency at ≈242 kHz. For polarization level evaluations, the magnetic field was reduced to 5.7 mT to record the spectrum of a water sample of equal volume at the proton Larmor frequency of ≈242 kHz. As discussed in Supporting Information, by taking into account the ratio between the gyromagnetic factors ($\gamma_{1_H}/\gamma_{13_C} = 4$), the number of scans ($n_{H_2O}/n_{CPE} = 5000$), the concentrations scaled by the corresponding number of spins ($2C_{H_2O}/C_{CPE} = 2000$) and the integral ratios ($S_{13_C}/S_{1_H} = 0.3$), the enhancement factor with respect to an equivalent thermally ^{13}C polarized sample is about 12 million. By noting that $p_{13_C}(293\ \mathrm{K}, 22.6\mathrm{mT}) = p_{1_H}(293\ \mathrm{K}, 5.7\ \mathrm{mT}) = 19.8$ ppb, the level of ^{13}C polarization on the carboxylic carbon of the pyruvate precursor is evaluated to be 24 %. In small flip-angle pulse-acquire experiments in the low-field magnet, the large SNR (≈660) of the HP pyruvate precursor allowed us to probe the decay of the ^{13}C signal and estimate the spin-lattice relaxation time $T_1 \cong 135$ s, see Figure 3b.

Long longitudinal relaxation times are advantageous for preserving the polarization while further manipulations are applied to remove the organic solvent, filter the catalyst and finally achieve HP pyruvate in water at physiological conditions, as described in Supporting Information in a

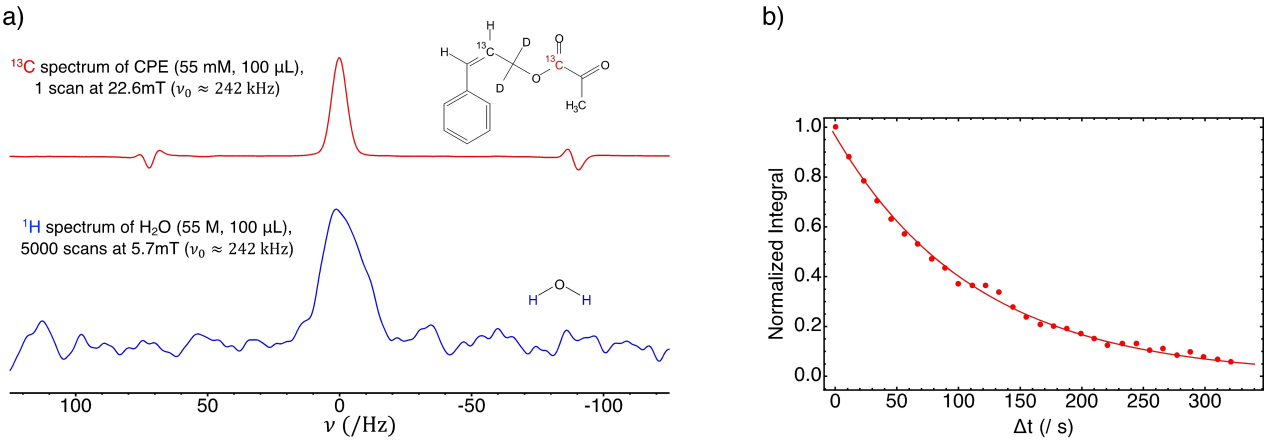

Figure 3. Hyperpolarization of the carboxylic carbon in the pyruvate precursor at 22.6 mT at 293 K. Panel a shows the HP ^{13}C signal of the precursor ($n_{CPE} = 1$ scan, $C_{CPE} = 55$ mM) at 22.6 mT versus the ^{1}H signal of H_2O ($n_{H_2O} = 5000$ scans, $C_{H_2O} = 55$ mM) at 5.7 mT on the same coil. The frequency scale of the spectra is relative to the corresponding Larmor frequency, $\nu_0 \approx 242$ kHz. The volume of the solutions was 100 µL in both cases. The ^{13}C polarization level is 24 %. Panel b shows the decay of the HP ^{13}C signal at 22.6 mT measured in a single-shot experiment, by using small flip-angle excitation pulses $\theta = 10°$ and a repetition time $T_R = 11$ s. The line represents the best fit to a mono-exponential decay (time constant $T_1^a = 114$ s). The actual spin-lattice relaxation time is calculated to $T_1 \cong 135$ s, using the formula $1/T_1 = 1/T_1^a + \ln(\cos\theta)/T_R$ to take into account the effect of the pulses.

slightly altered procedure to the one we have previously published.[25] Figure 4 shows the spectra of free HP [1-^{13}C]pyruvate in 200 µL neat water solution (after the purification and physiological adjustment steps) and its thermal counterpart. The polarization of the HP [1-^{13}C]pyruvate is 8%. The pyruvate concentration is evaluated to be 12 mM, by reference to an external calibration sample. As the acetone signals at 30 ppm and 207 ppm are below the noise level in the ^{13}C NMR thermal spectrum, we estimate conservatively the content to be less than 0.5 mg in the final solution (from an initial 100 µL volume). Acetone has relatively low toxicity compared to other organic solvents and is naturally present in the metabolism of mammals.[29–33] Blood acetone concentration in healthy humans is about 1 mg L^{-1} raising to 10 mg L^{-1} after exercise and in diabetic individuals.[33–35] Following exposure to 2000 ppm of acetone in air for 45 to 480 minutes, blood acetone levels at 2 mg mL^{-1} were found in rodents in vivo, with no adverse effects.[36] The ^{13}C NMR thermal spectrum displays no signal above the noise from the residual ^{13}C-labeled sidearm (cinnamyl alcohol), implying concentrations lower than 1 mM (≈30 µg). Pharmacological investigations of cinnamyl alcohol in non-clinical studies have shown no cytotoxic effects in vitro.[37,38] The residual rhodium concentration in the final solution was found to be below 45 µM (≈1µg) by Inductively Coupled Plasma Mass Spectroscopy (ICPMS) analysis, which corresponds to a 150-fold reduction from the value in the starting solution. Such amounts of rhodium appear to be well below the threshold of concern for in vitro biological studies and in vivo applications in rodents.[39,40]

The procedure was used to assess the metabolic turnover of pyruvate into lactate in HeLa cells, a prototypical cancer cell line. Figure 5 shows the course of the metabolic conversion of pyruvate into lactate as probed by ^{13}C NMR following the injection of the free HP [1-^{13}C]pyruvate neat water solution into an NMR tube containing 50 million HeLa cells suspended in cell culture medium at pH = 7.4. The signal-to-noise ratios (SNRs) of the pyruvate peak in the first spectrum ($\Delta t = 0$ s) and that of the lactate peak at its maximum ($\Delta t = 20$ s) are 18000 and 180, respectively. Notably, the carbon at position 2, which is present at natural abundance (1.1%), can be observed in the spectrum of the HP pyruvate.

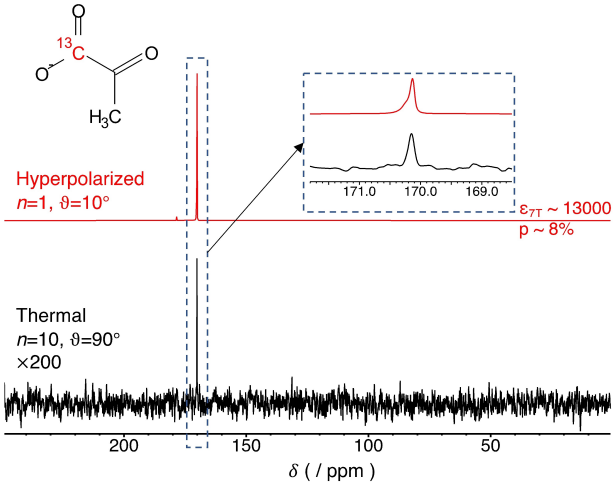

Figure 4. The spectrum of HP [1-^{13}C]pyruvate in biocompatible (isotonic, pH neutral, solvent-free and catalyst-free) water solution (number of scans $n = 1$, flip-angle $\theta = 10°$, in red) is shown above its thermal counterpart (number of scans $n = 10$, flip-angle $\theta = 90°$, scaled up by a factor 200, repetition time 300 s, in black). Spectra recorded at 7 T and 298 K. The region around 170 ppm, corresponding to the [1-^{13}C]pyruvate peak, is expanded in the inset for clarity.

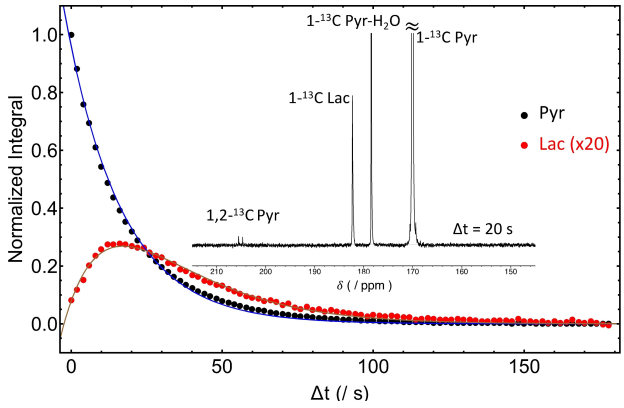

Figure 5. Real-time metabolism of pyruvate into lactate. After introducing HP [1-^{13}C]pyruvate in a suspension of HeLa cells, ^{13}C NMR spectra are collected using 10°-flip-angle pulses and a repetition time $T_R = 2$ s. The points represent the integrals of the NMR signals normalized to the area of the pyruvate peak (≈170 ppm) at the first point ($\Delta t = 0$ s). The integrals of the lactate peak (≈182 ppm) are multiplied by 20 for clarity. The lines represent the best fit to a unidirectional pyruvate-lactate conversion model, see Supporting Information for details. The inset shows the ^{13}C spectrum collected at $\Delta t = 20$ s. The peak at ≈179 ppm originates from the hydrated form of pyruvate. The doublet at ≈203 ppm originates from the ^{13}C in position 2 of [1,2-^{13}C$_2$]pyruvate, present at 1.1% natural abundance.

In comparison to the currently dominant hyperpolarization method (d-DNP), which requires dedicated high-field magnets, cryogenic and microwave technology, PHIP-based polarizers for NMR/MRI hold the promise to be affordable and portable and deliver fast polarization throughput.[41–47] In this article, we have introduced a field-independent pulsed heteronuclear-relayed PHIP-SAH method that achieves rapidly high levels of polarization on [1-^{13}C]pyruvate in a biocompatible catalyst-free water solution. Large *j*-couplings between the added hydrogen nuclei and an intermediate heteronucleus (one-bond ^{1}H-^{13}C in the precursor considered here) bring the spin system into weakly coupling conditions and induce PASADENA spin order in the hydrogenated substrate. The MINERVA pulse sequence has been used to transfer efficiently two-spin longitudinal order from para-H$_2$ into heteronuclear magnetization via the relaying ^{13}C nucleus. A rapid purification procedure finally leads to HP [1-^{13}C]pyruvate in catalyst-free water solutions at physiological conditions. In our current semi-automatic system, the full procedure is completed in less than 50 seconds, from the start of para-H$_2$ bubbling to the injection of the clean HP pyruvate solution. Specifically,

we obtained a ^{13}C polarization of 8% at 12 mM pyruvate concentration in clean water solutions (200 µl). Such figures appear adequate to perform in vitro studies, including ultrafast Fourier and Laplace spectroscopic modalities.[48–50] Here, we validated the method by monitoring the conversion of pyruvate into lactate in cancer cell lines.

The pulsed method proposed here is field-independent. It does not require highly-homogeneous magnetic fields and has been demonstrated on a portable low-field electromagnet. Compared to magnetic field cycling procedures where polarizations tend to diffuse over all the coupled spins, pulsed methods offer considerable control of the spin order transfer, so extending the set of PHIP precursors to complex spin systems, which can include deuterium nuclei and bridges to relay the para-H_2 spin order further away from the hydrogenation site. It is worth stressing that the synthesis of the precursor used here is straightforward and affordable within the context of isotopically labeled tracers for MRI.

Current state-of-the-art d-DNP polarizers epitomize 20 years of intense technological developments. Fully automated commercial systems can deliver ≈20–40%-polarized pyruvate solutions in 100–250 mM concentrations in batches of tens of milliliters for in vivo clinical applications.[51,52] However, high concentrations and large volumes are not always necessary or desirable. Volumes in the 100–500 µl range are well-suited for in vitro and preclinical in vivo (mouse models) HP-MR studies. The physiological concertation of pyruvate in blood lies in the 100–200 µM range. Concentrations above 10 mM can bias in vitro cell studies. Concentrations of 100 mM are adequate for in vivo preclinical MR studies. The upscaling of our method towards larger volumes and higher concentrations is a technical rather than a fundamental issue. For example, using 10 mm NMR tubes as reactors, we expect to deliver 0.5 mL clean solutions of HP pyruvate at 100 mM concentrations in the near future. We also anticipate that improved reaction conditions combined with a more automated setup will further reduce the polarization gap between our method and d-DNP.

We envision that portable systems, based on developments of the method proposed here, will become widespread for real-time assessment of metabolic processes in vitro and eventually in vivo.

Acknowledgements

We thank Dr. Lukas Kaltschnee for planning and setting up the customized para-H_2 generator used in these experiments. We thank the precision mechanics workshop of the Max Planck Institute of Multidisciplinary Sciences in Göttingen for machining the parts used to build the low field NMR probe. The authors are grateful to the Max Planck Society for generous funding. S. G. thanks the Deutsche Forschungsgemeinschaft (DFG) for funding (grants 418416679, 426677227 and 450146057). This project has received funding from the European Research Council (ERC) under the European Union's Horizon 2020 research and innovation program (Grant agreement No. 949180). Open Access funding enabled and organized by Projekt DEAL.

Conflict of Interest

The authors declare no conflict of interest.

Data Availability Statement

The data that support the findings of this study are available in the supplementary material of this article.

Keywords: Hyperpolarization · Magnetic Resonance · Metabolic Probes · Para-Hydrogen · Pyruvate

[1] S. E. Day, M. I. Kettunen, F. A. Gallagher, D. E. Hu, M. Lerche, J. Wolber, K. Golman, J. H. Ardenkjaer-Larsen, K. M. Brindle, *Nat. Med.* **2007**, *13*, 1382–1387.
[2] T. H. Witney, M. I. Kettunen, D. E. Hu, F. A. Gallagher, S. E. Bohndiek, R. Napolitano, K. M. Brindle, *Br. J. Cancer* **2010**, *103*, 1400–1406.
[3] S. E. Day, M. I. Kettunen, M. K. Cherukuri, J. B. Mitchell, M. J. Lizak, H. D. Morris, S. Matsumoto, A. P. Koretsky, K. M. Brindle, *Magn. Reson. Med.* **2011**, *65*, 557–563.
[4] S. J. Nelson, J. Kurhanewicz, D. B. Vigneron, P. E. Larson, A. L. Harzstark, M. Ferrone, M. van Criekinge, J. W. Chang, R. Bok, I. Park, G. Reed, L. Carvajal, E. J. Small, P. Munster, V. K. Weinberg, J. H. Ardenkjaer-Larsen, A. P. Chen, R. E. Hurd, L. I. Odegardstuen, F. J. Robb, J. Tropp, J. A. Murray, *Sci. Transl. Med.* **2013**, *5*, 198ra108.
[5] C. H. Cunningham, J. Y. C. Lau, A. P. Chen, B. J. Geraghty, W. J. Perks, I. Roifman, G. A. Wright, K. A. Connelly, *Circ. Res.* **2016**, *119*, 1177–1182.
[6] V. Z. Miloushev, K. L. Granlund, R. Boltyanskiy, S. K. Lyashchenko, L. M. DeAngelis, I. K. Mellinghoff, C. W. Brennan, V. Tabar, T. J. Yang, A. I. Holodny, R. E. Sosa, Y. W. W. Guo, A. P. Chen, J. Tropp, F. Robb, K. R. Keshari, *Cancer Res.* **2018**, *78*, 3755–3760.
[7] F. A. Gallagher, R. Woitek, M. A. McLean, A. B. Gill, R. M. Garcia, E. Provenzano, F. Riemer, J. Kaggie, A. Chhabra, S. Ursprung, J. T. Grist, C. J. Daniels, F. Zaccagna, M. C. Laurent, M. Locke, S. Hilborne, A. Frary, T. Torheim, C. Boursnell, A. Schiller, I. Patterson, R. Slough, B. Carmo, J. Kane, H. Biggs, E. Harrison, S. S. Deen, A. Patterson, T. Lanz, Z. Kingsbury, M. Ross, B. Basu, R. Baird, D. J. Lomas, E. Sala, J. Wason, O. M. Rueda, S. F. Chin, I. B. Wilkinson, M. J. Graves, J. E. Abraham, F. J. Gilbert, C. Caldas, K. M. Brindle, *Proc. Natl. Acad. Sci. USA* **2020**, *117*, 2092–2098.
[8] J. H. Ardenkjær-Larsen, B. Fridlund, A. Gram, G. Hansson, L. Hansson, M. H. Lerche, R. Servin, M. Thaning, K. Golman, *Proc. Natl. Acad. Sci. USA* **2003**, *100*, 10158–10163.
[9] C. R. Bowers, D. P. Weitekamp, *Phys. Rev. Lett.* **1986**, *57*, 2645–2648.
[10] C. R. Bowers, D. P. Weitekamp, *J. Am. Chem. Soc.* **1987**, *109*, 5541–5542.
[11] J. Natterer, J. Bargon, *Prog. Nucl. Magn. Reson. Spectrosc.* **1997**, *31*, 293–315.
[12] R. A. Green, R. W. Adams, S. B. Duckett, R. E. Mewis, D. C. Williamson, G. G. R. Green, *Prog. Nucl. Magn. Reson. Spectrosc.* **2012**, *67*, 1–48.
[13] F. Reineri, T. Boi, S. Aime, *Nat. Commun.* **2015**, *6*, 5858.

[14] E. Cavallari, C. Carrera, M. Sorge, G. Bonne, A. Muchir, S. Aime, F. Reineri, *Sci. Rep.* **2018**, *8*, 8366.
[15] E. Cavallari, C. Carrera, S. Aime, F. Reineri, *J. Magn. Reson.* **2018**, *289*, 12–17.
[16] E. Cavallari, C. Carrera, S. Aime, F. Reineri, *ChemPhysChem* **2019**, *20*, 318–325.
[17] E. Cavallari, C. Carrera, G. Di Matteo, O. Bondar, S. Aime, F. Reineri, *Front. Oncol.* **2020**, *10*, 497.
[18] F. Reineri, E. Cavallari, C. Carrera, S. Aime, *Magn. Reson. Mater. Phys. Biol. Med.* **2021**, *34*, 25–47.
[19] R. W. Adams, J. A. Aguilar, K. D. Atkinson, M. J. Cowley, P. I. P. Elliott, S. B. Duckett, G. G. R. Green, I. G. Khazal, J. Lopez-Serrano, D. C. Williamson, *Science* **2009**, *323*, 1708–1711.
[20] W. Iali, S. S. Roy, B. Tickner, F. Ahwal, A. J. Kennerley, S. B. Duckett, *Angew. Chem. Int. Ed.* **2019**, *58*, 10271–10275; *Angew. Chem.* **2019**, *131*, 10377–10381.
[21] I. Adelabu, P. TomHon, M. S. H. Kabir, S. Nantogma, M. Abdulmojeed, I. Mandzhieva, J. Ettedgui, R. E. Swenson, M. C. Krishna, T. Theis, B. M. Goodson, E. Y. Chekmenev, *ChemPhysChem* **2022**, *23*, 202100839.
[22] S. Korchak, S. Mamone, S. Gloggler, *ChemistryOpen* **2018**, *7*, 672–676.
[23] S. Korchak, S. J. Yang, S. Mamone, S. Gloggler, *ChemistryOpen* **2018**, *7*, 344–348.
[24] S. Korchak, M. Emondts, S. Mamone, B. Blumich, S. Gloggler, *Phys. Chem. Chem. Phys.* **2019**, *21*, 22849–22856.
[25] Y. Ding, S. Korchak, S. Mamone, A. P. Jagtap, G. Stevanato, S. Sternkopf, D. Moll, H. Schroeder, S. Becker, A. Fischer, E. Gerhardt, T. F. Outeiro, F. Opazo, C. Griesinger, S. Glöggler, *Chem. Methods* **2022**, 202200023.
[26] W. H. Koppenol, P. L. Bounds, C. V. Dang, *Nat. Rev. Cancer* **2011**, *11*, 325–337.
[27] O. Warburg, *Naturwissenschaften* **1924**, *12*, 1131–1137.
[28] S. Korchak, A. P. Jagtap, S. Gloggler, *Chem. Sci.* **2021**, *12*, 314–319.
[29] *Toxicological Profile for Acetone*, Agency for Toxic Substances and Disease Registry. U.S. Department of Health and Human Services, Public Health Service., Atlanta, GA (USA), **2021**.
[30] A. E. Koehler, E. Windsor, E. Hill, *J. Biol. Chem.* **1941**, *140*, 811–825.
[31] D. L. Coleman, *Proc. Natl. Acad. Sci. USA* **1980**, *77*, 290–293.
[32] J. P. Casazza, M. E. Felver, R. L. Veech, *J. Biol. Chem.* **1984**, *259*, 231–236.
[33] M. P. Kalapos, *Biochim. Biophys. Acta Gen. Subj.* **2003**, *1621*, 122–139.
[34] G. Wang, G. Maranelli, L. Perbellini, E. Raineri, F. Brugnone, *Int. Arch. Occup. Environ. Health* **1994**, *65*, 285–289.
[35] A. W. Jones, A. Sagarduy, E. Ericsson, H. J. Arnqvist, *J. Anal. Toxicol.* **1993**, *17*, 182–185.
[36] D. Dietz, *Toxic Rep. Ser.* **1991**, *3*, 1–38.
[37] Y. H. Kang, I. J. Yang, K. G. Morgan, H. M. Shin, *Exp. Mol. Med.* **2012**, *44*, 749–755.
[38] A. B. Monteiro, H. H. N. de Andrade, C. F. B. Felipe, R. N. de Almeida, *Rev. Bras. Farmacogn.* **2021**, *31*, 16–23.
[39] H. R. Chan, P. Bhattacharya, A. Imam, A. Freundlich, T. Tran, W. H. Perman, A. P. Lin, K. Harris, E. Y. Chekmenev, M. Ingram, B. D. Ross, in *2009 ISMRM Annual Meeting Proceedings*, *Vol. 17*, Honululu, **2009**, p. 2448.
[40] I. Iavicoli, V. Leso, L. Fontana, A. Marinaccio, A. Bergamaschi, E. J. Calabrese, *Chemosphere* **2014**, *104*, 120–125.
[41] J. B. Hövener, E. Y. Chekmenev, K. C. Harris, W. H. Perman, L. W. Robertson, B. D. Ross, P. Bhattacharya, *Magn. Reson. Mater. Phys. Biol. Med.* **2009**, *22*, 111–121.
[42] F. Reineri, A. Viale, S. Ellena, T. Boi, V. Daniele, R. Gobetto, S. Aime, *Angew. Chem. Int. Ed.* **2011**, *50*, 7350–7353; *Angew. Chem.* **2011**, *123*, 7488–7491.
[43] K. W. Waddell, A. M. Coffey, E. Y. Chekmenev, *J. Am. Chem. Soc.* **2011**, *133*, 97–101.
[44] S. Kadlecek, V. Vahdat, T. Nakayama, D. Ng, K. Emami, R. Rizi, *NMR Biomed.* **2011**, *24*, 933–942.
[45] R. Borowiak, N. Schwaderlapp, F. Huethe, T. Lickert, E. Fischer, S. Bar, J. Hennig, D. von Elverfeldt, J. B. Hovener, *Magn. Reson. Mater. Phys. Biol. Med.* **2013**, *26*, 491–499.
[46] A. M. Coffey, R. V. Shchepin, M. L. Truong, K. Wilkens, W. Pham, E. Y. Chekmenev, *Anal. Chem.* **2016**, *88*, 8279–8288.
[47] A. B. Schmidt, C. R. Bowers, K. Buckenmaier, E. Y. Chekmenev, H. de Maissin, J. Eills, F. Ellermann, S. Gloggler, J. W. Gordon, S. Knecht, I. V. Koptyug, J. Kuhn, A. N. Pravdivtsev, F. Reineri, T. Theis, K. Them, J. B. Hovener, *Anal. Chem.* **2022**, *94*, 479–502.
[48] S. Ahola, V. V. Zhivonitko, O. Mankinen, G. Zhang, A. M. Kantola, H. Y. Chen, C. Hilty, I. V. Koptyug, V. V. Telkki, *Nat. Commun.* **2015**, *6*, 8363.
[49] G. Zhang, S. Ahola, M. H. Lerche, V. V. Telkki, C. Hilty, *Anal. Chem.* **2018**, *90*, 11131–11137.
[50] O. Mankinen, V. V. Zhivonitko, A. Selent, S. Mailhiot, S. Komulainen, N. L. Prisle, S. Ahola, V. V. Telkki, *Nat. Commun.* **2020**, *11*, 3251.
[51] H. Y. Chen, P. E. Z. Larson, J. W. Gordon, R. A. Bok, M. Ferrone, M. van Criekinge, L. Carvajal, P. Cao, J. M. Pauly, A. B. Kerr, I. Park, J. B. Slater, S. J. Nelson, P. N. Munster, R. Aggarwal, J. Kurhanewicz, D. B. Vigneron, *Magn. Reson. Med.* **2018**, *80*, 2062–2072.
[52] H. Qin, S. Tang, A. M. Riselli, R. A. Bok, R. Delos Santos, M. van Criekinge, J. W. Gordon, R. Aggarwal, R. Chen, G. Goddard, C. T. Zhang, A. Chen, G. Reed, D. M. Ruscitto, J. Slater, R. Sriram, P. E. Z. Larson, D. B. Vigneron, J. Kurhanewicz, *Magn. Reson. Med.* **2022**, *87*, 138–149.

Manuscript received: May 1, 2022
Accepted manuscript online: June 20, 2022
Version of record online: July 14, 2022